Draft version November 2, 2021
Typeset using LaTeX twocolumn style in AASTeX631

Effective drag in rotating, poorly conducting plasma turbulence

Santiago J. Benavides [1], Keaton J. Burns [2,3], Basile Gallet [4] and Glenn R. Flierl [1]

[1] Department of Earth, Atmospheric, and Planetary Sciences, Massachusetts Institute of Technology, Cambridge, MA 02139, USA
[2] Department of Mathematics, Massachusetts Institute of Technology, Cambridge, MA 02139, USA
[3] Center for Computational Astrophysics, Flatiron Institute, New York, NY 10010, USA
[4] Université Paris-Saclay, CNRS, CEA, Service de Physique de l'Etat Condensé, 91191 Gif-sur-Yvette, France

ABSTRACT

Despite the increasing sophistication of numerical models of hot Jupiter atmospheres, the large time-scale separation required in simulating the large range in electrical conductivity between the dayside and nightside has made it difficult to run fully consistent magnetohydrodynamic (MHD) models. This has led many studies to resort to drag parametrizations of MHD. In this study, we revisit the question of the Lorentz force as an effective drag by running a series of direct numerical simulations of a weakly rotating, poorly conducting flow in the presence of a misaligned, strong background magnetic field. We find that the drag parametrization fails once the time-scale associated with Lorentz force becomes shorter than the dynamical time-scale in the system, beyond which the effective drag coefficient remains roughly constant, despite orders-of-magnitude variation in the time-scale. We offer an improvement to the drag parametrization by considering the relevant asymptotic limit of low conductivity and strong background magnetic field, known as the quasi-static MHD approximation of the Lorentz force. This approximation removes the fast time-scale associated with magnetic diffusion, but retains a more complex version of the Lorentz force, which could be utilized in future numerical models of hot Jupiter atmospheres.

Keywords: Astrophysical fluid dynamics(101) — Exoplanet atmospheres(487) — Magnetohydrodynamics(1964) — Hot Jupiters(753)

1. INTRODUCTION

Hot Jupiters (HJs) are gas giant exoplanets with masses similar to that of Jupiter, who orbit close enough to their host star that they are generally considered to be tidally locked (Seager 2010; Heng & Showman 2015). The proximity to their host stars is also expected to partially ionize the upper atmospheres of HJs, leading to the interaction between the atmospheric flows and any present magnetic fields (Batygin & Stevenson 2010; Perna et al. 2010a,b; Koskinen et al. 2010; Menou 2012; Koskinen et al. 2014). Their relatively large profile when obscuring their host star, as well as their short orbital periods, make them ideal candidates for transiting observations. In the last two decades, these observations have given us access to a great amount of information about their atmospheres, including some insight into their atmospheric dynamics – indirectly via hot spot migrations (Knutson et al. 2007, 2008; Zellem et al. 2014) and more directly using the blue-shifting of spectra observed at the terminators (Louden & Wheatley 2015; Ehrenreich et al. 2020). Their discovery, and subsequent observation of atmospheric dynamics, prompted the creation of a whole sub-field devoted to the numerical modeling of the atmospheres of HJs and their close relatives. These models range in sophistication and intent, from quasi-two-dimensional shallow water models (Cho et al. 2003; Langton & Laughlin 2007; Cho 2008; Showman & Polvani 2011; Heng & Workman 2014; Hindle et al. 2019) to three-dimensional general circulation models (GCMs) (Showman & Guillot 2002; Dobbs-Dixon & Lin 2008; Showman et al. 2009; Menou & Rauscher 2009; Perna et al. 2010a; Rauscher & Menou 2010; Heng et al. 2011; Rauscher & Menou 2013; Batygin et al. 2013; Rogers & Komacek 2014; Rogers & Showman 2014; Rogers & McElwaine 2017).

Corresponding author: Santiago J. Benavides
santib@mit.edu

One of the largest obstacles in modeling these atmospheres is the large conductivity contrast between the dayside and the nightside, due to the large differences in temperature (Perna et al. 2010a; Rogers & Komacek 2014; Heng & Showman 2015). The time scale of diffusion for induced magnetic fields is proportional to this conductivity, resulting in numerical models needing to resolve small time scales in the nightside, along with large time scales to capture large-scale structures in the atmosphere. Very large time-scale separations can be impractical for numerical simulations, and, as a result, many modelers resort to a parametrization of magnetic effects that doesn't directly resolve the magnetic diffusion time-scale. The most common approach begins by assuming that any induced magnetic field is a small, rapidly diffusing perturbation around a strong background magnetic field. This leads to a time-scale associated with the Lorentz force that is proportional to $\sigma_e^{-1}B_0^{-2}$, where σ_e is the electrical conductivity and B_0 is the strength of the background magnetic field (Davidson 1995, 2013; Knaepen & Moreau 2008). Modelers then substitute the Lorentz force with a drag term with an associated time-scale $\tau_{drag} \propto \sigma_e^{-1}B_0^{-2}$ (Perna et al. 2010a; Menou 2012; Rauscher & Menou 2012; Komacek & Showman 2016; Koll & Komacek 2018; Kreidberg et al. 2018; Arcangeli et al. 2019), which can also vary in space (Rauscher & Menou 2013; Beltz et al. 2021). For small values of σ_e the resulting drag time-scale is not restrictive for the numerics. Studies that have implemented what is dubbed as 'MHD drag' have found that the structure of the atmospheric circulation significantly changes when the drag time-scale is similar to or smaller than the relevant dynamical time-scale.

There are, however, reasons to question the validity of MHD drag. Recent attempts at modeling the full MHD equations in 3D GCMs, albeit with some simplifications, have shown that, although magnetic effects do reduce the strength of atmospheric jets (as a drag would), they also cause different morphological changes in the flow which make the authors question whether the correct prescription is a drag (Rogers & Komacek 2014). Furthermore, the authors find that the Ohmic dissipation measured in their MHD models is more than an order of magnitude smaller than would be predicted by a drag term. In an independent study, Heng & Workman (2014) arrive at a similar conclusion about MHD drag by studying the shallow water MHD model. See also Potherat & Klein (2017) for a similar discussion in the context of MHD experiments. Indeed, as we'll see in the next section, when considering the approximation of the Lorentz force in the relevant limits of low conductivity and large background magnetic field, one can show that a drag-like term appears in two-dimensional flows, but in three-dimensional flows this is not the case (Davidson 1995, 2013). Whether this approximation can be further reduced to a drag is unclear. The uncertainty of both the drag time-scale as well as the validity of the drag prescription itself, combined with their significant effects on the atmospheric circulation, make this a central issue in the modeling of HJ atmospheres and impacts our understanding and expectation of their atmospheric circulation.

In this study we revisit the question of the Lorentz force as an effective drag. In section 2 we consider an approximation to the full MHD equations in the relevant limits of low conductivity and strong background magnetic field, called quasi-static MHD (QMHD). In particular, we focus on the form of the approximate Lorentz force and discuss its properties and potential relation to a drag-like term, whose validity we quantify using an effective drag coefficient. In section 3 we describe the numerical setup and introduce an integral length-scale along the magnetic field, as a measure of the anisotropy in the flow. Then, in section 4 we measure the anisotropy and effective drag coefficient in a series of direct numerical simulations of QMHD turbulence in an idealized setup. We find that the drag parametrization works well for runs in which the dynamical time-scale is shorter than that which is associated with the Lorentz force. Beyond this, when the Lorentz force is sufficiently strong, the flow becomes anisotropic and the effective drag coefficient levels off. Finally, in section 5 we summarize our results and propose QMHD as an intermediate model, bridging the gap between the simplicity of a drag and the complexity of the full MHD equations, to be used in future GCMs of HJs.

2. ROTATING, WEAKLY CONDUCTING MHD

We aim to keep our fluid description of HJ atmospheres as simple as possible in an effort to focus purely on the dynamical effects of the Lorentz force. This means we will be ignoring many realistic features of HJ atmospheres, including stratification, radiation, compressibility, and kinetic plasma effects. Given their moderate temperatures, HJ atmospheres are also likely partially ionized (Batygin & Stevenson 2010; Perna et al. 2010a; Koskinen et al. 2014). However, except at very low pressures, the ions and neutrals are expected to be highly coupled due to collisions, meaning that a single-fluid description is an appropriate characterization (Perna et al. 2010a; Benavides & Flierl 2020). We thus begin by considering incompressible magnetohydrodynamics (MHD) with uniform density, subject to rotation $\mathbf{\Omega}$ and a uniform, steady background magnetic field

$\boldsymbol{B_0}$. Further simplifications will be achieved by considering two relevant limits, low electrical conductivity, and a strong background magnetic field field.

The effect of electrical conductivity on the dynamics is quantified by the magnetic Reynolds number Re_m, a dimensionless parameter comparing the magnetic diffusion time-scale to the time-scale associated with the evolving flow (Davidson 2013). We define $Re_m = \ell u/\eta$, where $\eta = (\mu_0\sigma_e)^{-1}$ is the magnetic diffusivity, μ_0 is the magnetic permeability, ℓ is a dominant length-scale of the flow, and u is a velocity scale. If $Re_m \ll 1$, the diffusion and dissipation of induced magnetic fields is significant. Hot Jupiters with daysides cooler than roughly 1800 K are expected to have magnetic Reynolds number smaller than one throughout most of their atmospheres (Perna et al. 2010a), although this assumption could break down on the dayside of the hotter HJs at lower pressures (Menou 2012; Rogers & Komacek 2014). Importantly, dynamo instabilities are not present in flows with $Re_m \lesssim 1$, and thus do not convert kinetic energy to magnetic energy, resulting in a decaying induced magnetic field and a negligible Lorentz force, $\boldsymbol{j} \times \boldsymbol{b}$, where $\boldsymbol{j} = \mu_0^{-1}\nabla \times \boldsymbol{b}$.

However, in the presence of a background magnetic field (from a deeper dynamo region or from the host star), the flow can act to exchange kinetic for magnetic energy by impinging on this field and producing induced currents and magnetic fields. In a flow with low conductivity, the strength of this induced magnetic field scales like $b \sim Re_m B_0$, and thus the Lorentz force scales like $|\boldsymbol{j}\times(\boldsymbol{b}+\boldsymbol{B_0})| \sim Re_m B_0^2 \ell^{-1}\mu_0^{-1} \propto \sigma_e B_0^2$ (Davidson 1995, 2013; Knaepen & Moreau 2008). This is the origin of τ_{drag} discussed in Section 1. We estimate the relevance of the Lorentz force in the dynamics by comparing the strength of the Lorentz force to the nonlinear advection term in the momentum equation, giving us our main control parameter in this study, known as the *interaction parameter*:

$$N \equiv Re_m \frac{B_0^2}{\mu_0 \rho u^2} = \frac{\sigma_e \ell B_0^2}{\rho u}. \tag{1}$$

Despite $Re_m \ll 1$, if $B_0/(\sqrt{\mu_0\rho}u)$ is large enough such that $N \gtrsim 1$, then the Lorentz force can significantly affect the dynamics. Some recent studies have estimated magnetic field strengths for HJs and found magnitudes similar to that of Jupiter, but possibly up to 50 times greater for larger HJs, suggesting that this limit could be relevant for some HJs (Reiners & Christensen 2010; Yadav & Thorngren 2017; Rogers 2017; Hindle et al. 2021).

Flows with $Re_m \ll 1$ and $N \sim \mathcal{O}(1)$ have the distinct property that the magnetic field is 'instantly' diffused away, yet the Lorentz force is *not* negligible. This limit is referred to as the *quasi-static* approximation to MHD (which we call 'QMHD' henceforth) (Moffatt 1967; Sommeria & Moreau 1982; Davidson 1995, 2013; Knaepen & Moreau 2008), and has been studied mainly in metallurgy and in MHD experiments due to the typically low conductivity of liquid metals (Alemany et al. 1979; Sommeria 1988; Gallet et al. 2009; Klein & Pothérat 2010; Pothérat & Klein 2014; Baker et al. 2018), although recent numerical studies on its turbulent properties and anisotropy have been done as well (Zikanov & Thess 1998; Burattini et al. 2008; Favier et al. 2010, 2011; Reddy & Verma 2014; Verma 2017). After nondimensionalizing the equations of MHD using the uniform density ρ, ℓ and u, and taking the limits above, one is left with a single dynamical equation for the velocity[1]:

$$\begin{aligned} \frac{\partial \boldsymbol{v}}{\partial t} + (\boldsymbol{v}\cdot\nabla)\,\boldsymbol{v} = &-\nabla p^* - Ro^{-1}\hat{\boldsymbol{x}}_\parallel^\Omega \times \boldsymbol{v} \\ &-N\nabla^{-2}(\hat{\boldsymbol{x}}_\parallel^{B_0}\cdot\nabla)^2\boldsymbol{v} + \boldsymbol{F}, \end{aligned} \tag{2}$$

where p^* is the total pressure modified by rotation and magnetic pressure, $Ro^{-1} \equiv 2\Omega\ell/u$ is the inverse Rossby number (quantifying the relative strength of the Coriolis force), $\hat{\boldsymbol{x}}_\parallel^\Omega$ and $\hat{\boldsymbol{x}}_\parallel^{B_0}$ are unit vectors in the direction of rotation and the background magnetic field, respectively, and $\boldsymbol{F}$ is a generic forcing term that can include dissipation such as viscosity and a body force (to be specified in Section 3). This equation is accompanied with the incompressibility condition $\nabla\cdot\boldsymbol{v} = 0$. The induced magnetic field can be found using a diagnostic relation:

$$\boldsymbol{b} = -\nabla^{-2}\left(\hat{\boldsymbol{x}}_\parallel^{B_0}\cdot\nabla\right)\boldsymbol{v}, \tag{3}$$

which would be $\boldsymbol{b} = -\nabla^{-2}\left(\boldsymbol{B_0}\cdot\nabla\right)\boldsymbol{v}/\eta$ in dimensional variables.

In QMHD, the Lorentz force operator,

$$\mathcal{L}(\boldsymbol{v}) \equiv -N\nabla^{-2}(\hat{\boldsymbol{x}}_\parallel^{B_0}\cdot\nabla)^2\boldsymbol{v}, \tag{4}$$

acts to dissipate kinetic energy from any motion which varies along the direction of the background magnetic field. In two-dimensional flows, with an in-plane $\boldsymbol{B_0}$, it can be shown that $\mathcal{L}(\boldsymbol{v})$ becomes $\mathcal{L}_{2D}(\boldsymbol{v}) = -N\boldsymbol{v}_\perp^{B_0}$, where $\boldsymbol{v}_\perp^{B_0}$ is the projection of the velocity perpendicular to the background field (Davidson 1995, 2013). These two properties would, at first glance, seem to justify the use of a drag parametrization. However, most HJs are expected to be tidally locked, resulting in order one Rossby numbers (Seager (2010), Part V), which is not

[1] Care must be taken if considering a spatially-dependent background magnetic field $\boldsymbol{B_0}(\boldsymbol{x})$, as the end result will not be the same. See the discussion in Section 5.

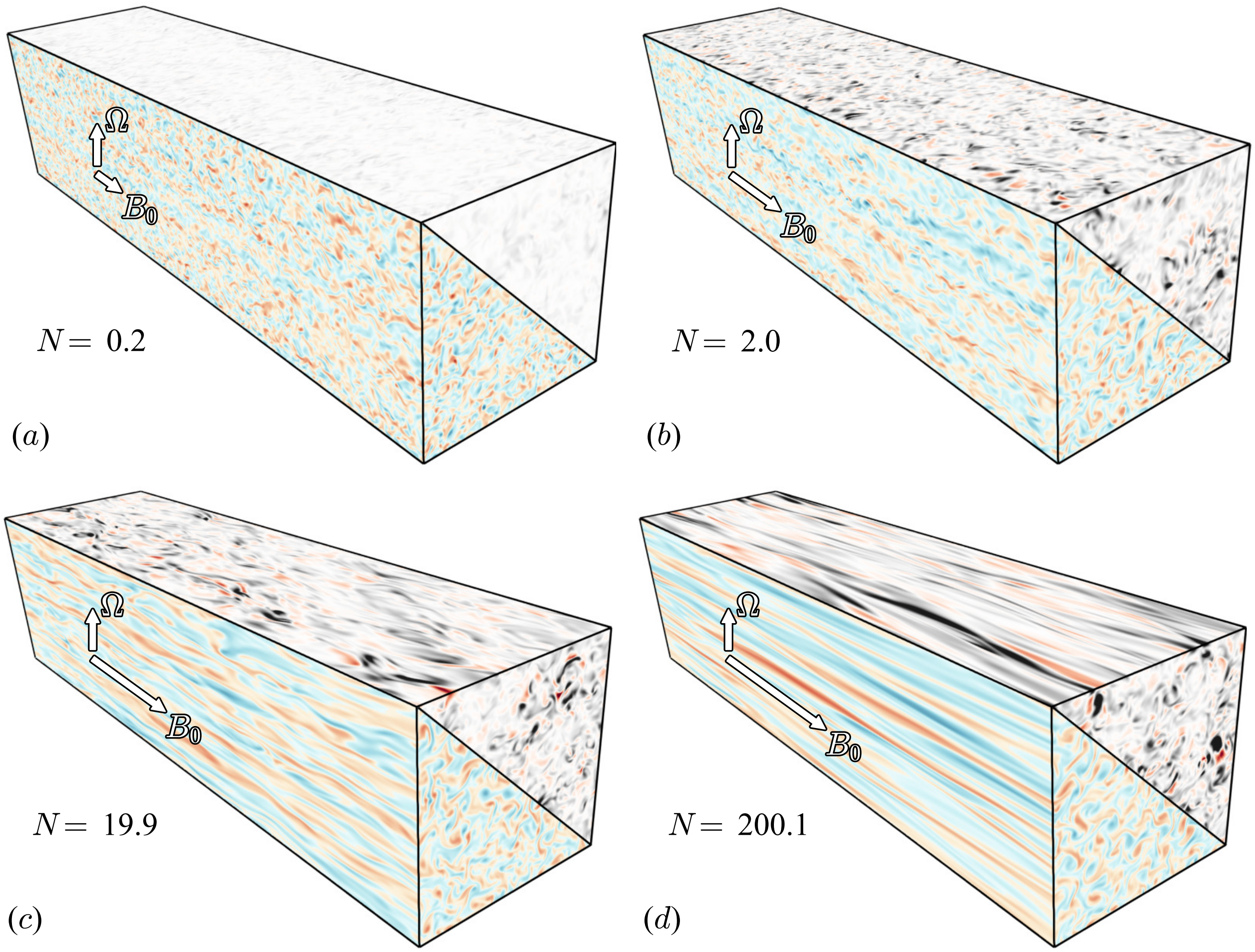

Figure 1. Snapshots from the $L_x = 8\pi L$ runs (Table 1) of the field-aligned vorticity $\omega = \hat{x} \cdot (\nabla \times \boldsymbol{v})$ (lower left, in blue and red) and the Ohmic dissipation $\boldsymbol{v} \cdot \mathcal{L}(\boldsymbol{v})$ (upper right, in black and red) for increasing values of the interaction parameter N (equation (1)). Figures 1(b)-(d) represent runs with approximately equal values of Ohmic dissipation and D_{eff} (equation (5)). The red colors represent positive values whereas the blue and black represent negative values. All snapshots use the same colorbar scale for each given field.

low enough for strong two-dimensionalization of these flows. In three dimensions, the Lorentz force $\mathcal{L}(\boldsymbol{v})$ acts to create *anisotropy* in the flow by removing energy from motions that vary along the magnetic field, but does not affect motions that are invariant along that direction. This is in sharp contrast to a drag in which any motion is affected equally and in an isotropic way.

Despite these differences, $\mathcal{L}$ does remove energy from the flow, and has the dimensions of an inverse time-scale, so there is hope that the much simpler approximation of $\mathcal{L}$ as a drag could be valid in certain regimes. In order to investigate this in a quantitative way, we introduce an *effective drag coefficient* D_{eff},

$$D_{eff} \equiv -\frac{\langle \boldsymbol{v} \cdot \mathcal{L}(\boldsymbol{v}) \rangle}{\langle |\boldsymbol{v}|^2 \rangle}, \tag{5}$$

where $\langle \cdot \rangle$ denotes a temporal and spatial average at steady state. If $\mathcal{L}$ does indeed act like a drag, then $D_{eff} \approx N$, as we would expect. However, if this is not the case, then D_{eff} will deviate from N. $\langle \boldsymbol{v} \cdot \mathcal{L}(\boldsymbol{v}) \rangle$ is the Ohmic dissipation rate, so that equation (5) represents the ratio of Ohmic dissipation to (twice) the kinetic energy in the flow.

In the next section we introduce a series of direct numerical simulations of QMHD turbulence which we use to investigate how $\mathcal{L}$ acts to create anisotropy, and how that, in turn, affects the validity of $\mathcal{L}$ as a drag. *How does the effective drag coefficient depend on N?*

3. METHODS

We performed direct numerical simulations of the QMHD system, equation (2), in a triply-periodic domain using a modified version of the Geophysical High-

Order Suite for Turbulence (GHOST) (Mininni et al. 2011; Benavides 2021), a pseudo-spectral code with a fourth-order Runge–Kutta scheme for time integration and a two-thirds dealiasing rule. The generic forcing term $\boldsymbol{F}$ comprised of a 'hyper'-viscous term, $-\nu\nabla^4\boldsymbol{v}$, which acts to dissipate energy at the smallest scales, and a body forcing term $\boldsymbol{f}$, which is random (white-in-time) and injects energy into the flow at a constant rate f_0^2 and at a single length-scale ℓ_f. The hyper-viscosity lets us use lower resolutions while maintaining numerical accuracy, and has been shown to have no significant effect on the turbulent properties of 3D turbulence as long as the power of the gradient is small enough, as is the case here (Agrawal et al. 2020).

The axis of rotation was chosen to be in the vertical direction $\hat{\boldsymbol{x}}_\parallel^\Omega = \hat{\boldsymbol{z}}$, whereas the direction of the background magnetic field was chosen to be perpendicular to it, in the x-direction, $\hat{\boldsymbol{x}}_\parallel^{B_0} = \hat{\boldsymbol{x}}$. The misalignment between the rotation axis and background field is supposed to reflect a generic case, since there is no reason to expect alignment between the two outside the dynamo region (e.g., a dipole field from the interior dynamo region). In some cases misaligned rotation and background field can have significant consequences on the dynamics (Benavides et al. 2021), so we performed runs at other misalignment angles, θ, defined to be the angle the background field makes with the rotation. These runs show that our results do not depend strongly on the misalignment angle.

Since $\mathcal{L}$ dissipates motion that varies along x, we expect anisotropy to develop in our domain, manifested by structures along the x-direction which are larger than in the perpendicular directions. In order to accommodate the form of $\mathcal{L}$, and the resulting anisotropy, we make a few specific choices in our implementation. First of all, we perform the same set of runs for various values of L_x, the domain size in the x-direction. The domain size in the perpendicular direction is fixed at $L_y = L_z = 2\pi L$, whereas we perform sets of runs with $L_x = 2\pi L, 4\pi L$ and $8\pi L$. Second, the forcing function $\boldsymbol{f}$ 'stirs' the fluid in a manner that does not vary along the x-direction, so that the forcing does not project onto $\mathcal{L}$, which would immediately dissipate the energy being forced. Since such two-dimensional forcing results in three-dimensional instabilities, the resulting flow is still approximately isotropic when $N \ll 1$.

The numerical model is nondimensionalized by L and f_0, such that the domain size in the perpendicular directions is 2π and the forcing function has an injection rate equal to 1. In all of our runs, we have $\nu = 2\times10^{-6}$, $\Omega = 2$, and $\ell_f = 2\pi/k_f$, where $k_f = 9$ (we randomly force modes $\boldsymbol{k}$ such that $8 < |\boldsymbol{k}| < 10$, making $k_f = 9$).

L_x	Nx	θ	N	# of Runs
$2\pi L$	256	$30°, 60°, 90°$	$2\times10^{-3} - 200$	33
$4\pi L$	512	$90°$	$2\times10^{-1} - 300$	8
$8\pi L$	1024	$90°$	$2\times10^{-1} - 600$	8

Table 1. A summary of the runs performed for this work. All runs have (in simulations units, nondimensionalized by L and f_0) $\nu = 2\times10^{-6}$, $\Omega = 2$, and $\ell_f = 2\pi/k_f$, where $k_f = 9$. This corresponds to an inverse Rossby number of $Ro^{-1} = 1.98$, and an 'effective' Reynolds number of $Re = 14973$. Nx represents the number of grid points in the x-direction. All runs have 256 grid points in both y and z directions.

The dominant length-scale in the problem is $\ell = \ell_f/2$, if we consider the size of a typical vortex produced by the forcing. The velocity scale is defined using the four-fifths law, $u = (f_0^2\ell)^{1/3} = \ell^{1/3} = (\pi/9)^{1/3}$. These values of ℓ and u result in an inverse Rossby number of $Ro^{-1} = 1.98$, and an 'effective' Reynolds number of $Re = 14973$, where $Re \equiv u\ell^3/\nu$ is based on the hyper-dissipation used in our model. All of our runs have a resolution of 256 in each direction perpendicular to the background field. See Table 1 for a list of the runs performed in our study. Note that, although we are varying N over many orders of magnitude, the magnetic Reynolds number remains much smaller than one and $B_0/(\sqrt{\mu_0\rho}u)$ much larger than one, which are the assumptions of QMHD.

Each simulation is run until a steady-state is reached, at which point the time-averages are taken. For each run we calculate the effective drag coefficient D_{eff}, as well as an integral length-scale in the x-direction, defined as:

$$\overline{\ell_x} = \left(\frac{\int (k_x/2\pi)E(k_x)\ dk_x}{\int E(k_x)\ dk_x}\right)^{-1}, \tag{6}$$

where $E(k_x)$ is the time-averaged, one-dimensional energy spectrum in the x-direction. Note that these integrals also include contributions from the $k_x = 0$ mode. $\overline{\ell_x}$ gives an estimate of the dominant length-scale in the x-direction (in units of L), and will be used as a quantitative measure of anisotropy developing in the domain. In an isotropic system we would expect $\overline{\ell_x} \sim \ell_f$.

4. RESULTS

4.1. *Anisotropy*

Our simulations show that significant anisotropy develops in the flow once $N \gtrsim 1$ (Figures 1 and 2). For $N < 1$ the Lorentz force is negligible and does not affect the dynamics, resulting in approximately isotropic flow with $\overline{\ell_x} \approx 1.33\ell_f$. The slightly-larger-than-one prefactor likely comes from the fact that the forced two-

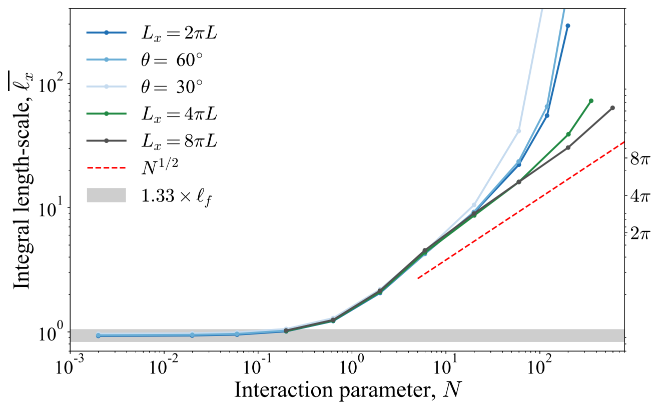

Figure 2. The integral length-scale $\overline{\ell_x}$ (equation (6)), in units of L, as a function of the interaction parameter N (equation (1)), for various box sizes and misalignment angles. In gray we show 1.33 times the forcing length-scale range. Anisotropy develops once $N > 1$, and this does not depend on the domain size or misalignment angle. For $N > 1$ and sufficiently large domains which do not suffer from finite size effects (when $\overline{\ell_x} < L_x$, see axis on right), we find that $\overline{\ell_x} \sim N^{1/2}$ (red, dashed line).

dimensional flow is unstable to three-dimensional perturbations at many length-scales. Another thing to note is that the onset of anisotropy does not depend on domain size or misalignment angle.

As N increases beyond one, the Lorentz force dissipates structures that vary long the x direction, acting more strongly on those with small length-scales. This results in more elongated structures as N increases (Figure 1). $\overline{\ell_x}$ grows until all $k_x > 0$ modes are stable and the flow becomes exactly two-dimensional at a critical value N_{2D}, where $N_{2D} \propto L_x^2$ (Zikanov & Thess 1998; Favier et al. 2010; Thess & Zikanov 2007; Gallet & Doering 2015). The effects of N_{2D} are seen for $N < N_{2D}$ – finite domain size effects appear when $\overline{\ell_x} \gtrsim L_x$ (Figures 2). The exact two-dimensionalization will also depend on the Reynolds number, with N_{2D} increasing with Re (Gallet & Doering 2015). Given the large physical extent and Reynolds numbers of astrophysical flows, we don't expect the two-dimensionalization to be a relevant physical phenomenon. Therefore, to avoid these effects which we believe to be irrelevant for our motivation, we consider larger domains, which allow us to push N_{2D} to larger values, and therefore begin to approach the astrophysically-relevant regimes.

The runs on larger domains reveal a power-law dependence of $\overline{\ell_x}$ with N, with an observed anisotropy scaling of $\overline{\ell_x} \sim N^{1/2}$ (Figure 2). This agrees with previous scaling predictions, such as that by Sommeria & Moreau (1982) who considered $\mathcal{L}$ as an along-field diffusion $\mathcal{L}(\boldsymbol{v}) \approx \mathcal{L}_{diff}(\boldsymbol{v}) = \kappa \partial_x^2 \boldsymbol{v}$, with $\kappa \sim \sigma B_0^2 \ell_\perp^2 / \rho$ and $\ell_\perp \sim \ell_f$ based on our forcing. In an eddy turnover time τ_{eddy}, motions with horizontal extent $\ell_\perp$ would diffuse vertically with a diffusion length of $\ell_x \sim \sqrt{\kappa \tau_{eddy}} \propto B_0 \ell_\perp \propto N^{1/2} \ell_\perp$. This scaling can also be arrived at by considering the wavenumbers whose turbulent timescales match that of the Lorentz force, and are therefore damped away. This gives $k\ u(k) \sim f_0^{2/3} k^{2/3} \sim N k_x^2/k^2$, resulting in $k_x^{-1} k_\perp^{4/3} \sim \ell_x / \ell_\perp^{4/3} \sim N^{1/2}$. The slightly different scaling for $\ell_\perp$ comes from the dependence of τ_{eddy} on $\ell_\perp$, based on 3D homogeneous and isotropic turbulence assumptions (Frisch 1995), which is not considered in the diffusivity argument.

For $1 \ll N < N_{2D}$ the anisotropy is such that the flow is almost two-dimensional (e.g., Figure 1 (d)). Previous studies looking at turbulent energy cascades have found that inverse energy cascades (associated with two-dimensional hydrodynamics) appear before exact two-dimensionalization (Alexakis 2011; Benavides & Alexakis 2017; Alexakis & Biferale 2018; Pouquet et al. 2019). However, in our runs we don't see any sign of an inverse cascade forming. This is due to the weak rotation in the z-direction, coupling the horizontal and out-of-plane velocities which results in a system with a forward cascade of energy (Benavides et al. 2021). If rotation were to be weaker, we would expect the formation of an inverse cascade. Indeed, this seems to be occurring for the $\theta = 30°$ run, where the projection of the rotation perpendicular to the background field is smaller, resulting in weaker in-plane rotation rate. The inverse cascade for this case results in larger horizontal scales $\ell_\perp$, which we believe pushes N_{2D} to lower values (Figure 2). On the other hand, for cases with very fast rotation, the Taylor-Proudman theorem would manifest itself as flow becoming invariant along the z-direction, resulting in a series of shear layers varying in the third direction, y (Benavides et al. 2021). This latter case might be more relevant for the transition regions of gas giant planets like Jupiter and Saturn, where the conditions for QMHD are also likely satisfied, but where rotation rates are significantly larger than those of HJs.

4.2. *Effective drag*

An increase in $\overline{\ell_x}$ implies a decrease in the x-derivative found in $\mathcal{L}$, thereby effectively lowering the Ohmic dissipation. However, the decrease in the x-derivative occurs as we increase N, which also appears in $\mathcal{L}$. What is the combined effect on D_{eff} of N increasing but the x-derivative decreasing? Figure 3 shows the effective drag coefficient D_{eff} as we vary the control parameter N. For $N < 1$, while the flow is approximately isotropic, we see a good agreement with $D_{eff} \propto N$, suggesting that

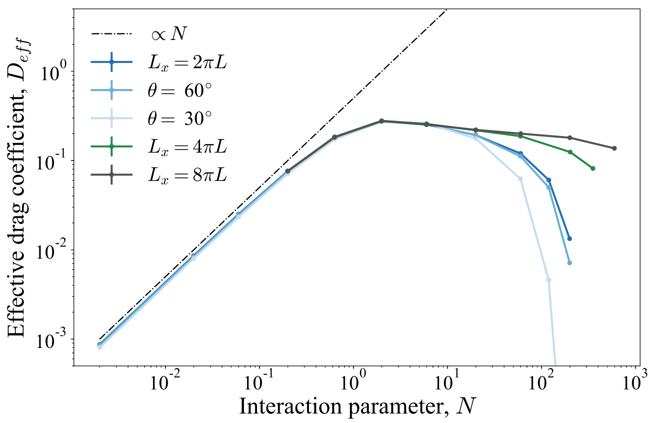

Figure 3. The effective drag coefficient D_{eff} (equation (5)) versus interaction parameter N (equation (1)), for various box sizes and misalignment angles. For $N < 1$, the effective drag coefficient seems to be proportional to N (black, dash-dotted line), suggesting a good agreement. However, the curve levels off and deviates significantly from the drag prediction by orders of magnitude when $N > 1$, independent of domain size and misalignment angle θ.

a drag-like parametrization could correctly capture the dynamics and Ohmic dissipation in this regime. However, as anisotropy develops for $N \gtrsim 1$, the structures that dissipate the most energy appear at larger scales (Figure 1) and D_{eff} begins to deviate from the one-to-one line. Much like the anisotropy, the deviation from the one-to-one line does not depend on the domain size or misalignment angle.

It is not clear *a priori* what the behavior of D_{eff} should be beyond this point. For the $L_x = 2\pi L$ runs, D_{eff} begins to decrease beyond $N \sim 1$. However, this is a result of the finite domain size and proximity to N_{2D}. By looking at successively larger L_x runs, we probe what would happen in a more realistic setting. Figure 3 suggests that, for large L_x, the effective drag coefficient D_{eff} levels off and remains roughly constant, despite orders of magnitude increase in N. We found that this behavior and value of D_{eff} does not depend strongly on Re. Figure 1 (b)-(d) shows snapshots of runs which have approximately the same effective drag coefficient, while representing three orders of magnitude for N. Structures change in such a way so as to keep D_{eff} roughly constant, given the increase in N.

Given our findings from Figure 2, we can see why this behavior is a result of the anisotropy scaling $\overline{\ell_x} \sim N^{1/2}$. Combining equations (4) and (5), we can re-frame D_{eff} as a weighted average of wavenumbers:

$$D_{eff} = N\overline{\left(\frac{k_x^2}{k^2}\right)}, \tag{7}$$

where $k^2 = k_x^2 + k_y^2 + k_z^2$. When $N > 1$, we would expect $k_x^2 < k_\perp^2 = k_y^2 + k_z^2$, so that we can replace k^2 with $k_\perp^2$ in equation (7). Assuming $k_\perp$ doesn't vary significantly, since the forcing remains the same and no large-scale structures form in the flow, we can approximate it with $k_\perp \sim 2\pi\ell_f^{-1}$. Finally, substituting $\overline{k_x^2} = 2\pi\overline{\ell_x}^{-2}$, we end up with the with:

$$D_{eff} \approx N\left(\frac{\overline{\ell_x}}{\ell_\perp}\right)^{-2} \sim NN^{-1} \sim \text{const.} \tag{8}$$

In other words, the effective drag coefficient is N divided by the anisotropy of the flow squared. Since we know how the anisotropy scales with N, we can get D_{eff} as a function of N, which in the end turns out to be a constant.

Recall that D_{eff} is proportional to the Ohmic dissipation rate, so that a levelling-off of D_{eff} also represents the same behavior for the Ohmic dissipation[2]. A similar plateauing behavior has been observed for the Ohmic dissipation in HJ GCM runs with increasing temperatures (Rogers & Komacek 2014). The authors attribute this to a change in dynamics as Re_m increases past one at lower pressures. However, they note that at higher pressures, and for some of the lower temperature runs where the plateau begins, Re_m is still low, so it's possible that the QMHD effects seen here might be present and partially responsible for what is observed.

5. CONCLUSIONS

In this study, we considered the turbulent dynamics of rotating MHD in the presence of a background magnetic field, in the combined limit of $Re_m \ll 1$ and $B_0/(u\sqrt{\mu_0\rho}) \gg 1$, termed quasi-static MHD (QMHD). Motivated by approaches used in the study of hot Jupiter (HJ) atmospheres, we have shown that a drag parametrization of the Lorentz force operator $\mathcal{L}$ fails once the ratio of the dynamical timescale to the Lorentz timescale, quantified by the interaction parameter N, is larger than one. This happens because the Lorentz force dissipates structures that vary along the background field, creating anisotropy in the flow, which in turn acts to reduce the Ohmic dissipation, thereby reducing the effective drag. The development of anisotropy with increasing N is such that the effective drag coefficient remains constant for $N > 1$, despite N varying by orders of magnitude. The levelling off of D_{eff} for $N > 1$ has significant implications for simulations parametrizing $\mathcal{L}$

[2] The kinetic energy is approximately the same for all runs here, partly due to the presence of a forward cascade. This might change in the case of weaker rotation and subsequent formation of an inverse cascade.

as a drag, since we see values of D_{eff} deviating by orders of magnitude from what would be predicted if one assumes $\mathcal{L} = \mathcal{L}_{drag} = -N$. This could also result in severely overestimating the amount of Ohmic dissipation, as well as misrepresenting the true dynamics of HJ atmospheres.

The main motivation for a drag parametrization of the Lorentz force comes from the restrictively small time scales associated with very large magnetic diffusivities (low electrical conductivity). The drag time-scale is much larger than the time-scale associated with magnetic diffusion, allowing modellers to bypass this problem. While we have found that a drag parametrization fails for $N > 1$, we want to emphasize that the same time-scale advantage exists in the QMHD limit, despite the more complicated form of the operator associated with the Lorentz force. This will hopefully motivate the use of the QMHD approximation in models of HJ atmospheres. Even for the case of a spatially-dependent background magnetic field or conductivity, its implementation would be straight forward if one considers separately the Lorentz force $\mu_0^{-1}(\nabla \times \boldsymbol{b}) \times \boldsymbol{B_0}(\boldsymbol{x})$ and the induced magnetic field $\boldsymbol{b} = -\nabla^{-2}(\eta(\boldsymbol{x})^{-1}\nabla\times(\boldsymbol{v}\times\boldsymbol{B_0}(\boldsymbol{x})))$. An alternative which might be easier to implement would be to approximate ∇^{-2} with some horizontal length-scale $\ell_\perp^2$, similar to what was done when considering $\mathcal{L}(\boldsymbol{v})$ as an along-field diffusivity, $\mathcal{L}(\boldsymbol{v}) \approx \mathcal{L}_{diff}(\boldsymbol{v}) = \kappa\partial_x^2\boldsymbol{v}$, with $\kappa \sim \sigma B_0^2\ell_\perp^2/\rho$ (Sommeria & Moreau 1982). Although the expression for $\mathcal{L}$ (equation (4)) would be modified in the presence of a spatially-dependent background magnetic field, we expect our results to hold for those cases, as well.

We thank Thaddeus D. Komacek for insightful discussions and helpful suggestions. This research was carried out in part during the 2019 Summer School at the Center for Computational Astrophysics, Flatiron Institute. The Flatiron Institute is supported by the Simons Foundation. SJB acknowledges funding from the National Aeronautics and Space Administration (Award Number: 80NSSC20K1367) issued through the Future Investigators in NASA Earth and Space Science and Technology (NNH19ZDA001N-FINESST) within the NASA Research Announcement (NRA): Research Opportunities in Space and Earth Sciences (ROSES-2019).

Software: Geophysical High-Order Suite for Turbulence (GHOST). Branch: pre-release-2, Commit: 979b9fee3425dd7836687ffe6acff66e41d7083f (Benavides 2021). Forked and modified from Mininni et al. (2011), see https://github.com/pmininni/GHOST.

REFERENCES

Agrawal, R., Alexakis, A., Brachet, M. E., & Tuckerman, L. S. 2020, Phys. Rev. Fluids, 5, 024601

Alemany, A., Moreau, R., Sulem, P. L., & Frisch, U. 1979, Journal de Mecanique, 18, 277

Alexakis, A. 2011, Phys. Rev. E, 84, 056330

Alexakis, A., & Biferale, L. 2018, Physics Reports, 767-769, 1

Arcangeli, J., Désert, J.-M., Parmentier, V., et al. 2019, A&A, 625, A136, doi: 10.1051/0004-6361/201834891

Baker, N. T., Pothérat, A., Davoust, L., & Debray, F. 2018, Phys. Rev. Lett., 120, 224502

Batygin, K., Stanley, S., & Stevenson, D. J. 2013, The Astrophysical Journal, 776, 53, doi: 10.1088/0004-637x/776/1/53

Batygin, K., & Stevenson, D. J. 2010, The Astrophysical Journal Letters, 714, L238. http://stacks.iop.org/2041-8205/714/i=2/a=L238

Beltz, H., Rauscher, E., Roman, M., & Guilliat, A. 2021, Exploring the Effects of Active Magnetic Drag in a GCM of the Ultra-Hot Jupiter WASP-76b. https://arxiv.org/abs/2109.13371

Benavides, S. J. 2021, GitHub repository, https://github.com/s-benavides/GHOST/tree/pre-release-2, Commit: 979b9fee3425dd7836687ffe6acff66e41d7083f

Benavides, S. J., & Alexakis, A. 2017, Journal of Fluid Mechanics, 822, 364–385, doi: 10.1017/jfm.2017.293

Benavides, S. J., Burns, K. J., Gallet, B., Cho, J. Y.-K., & Flierl, G. R. 2021, Inverse cascade suppression and shear layer formation in MHD turbulence subject to a guide field and misaligned rotation. https://arxiv.org/abs/2104.12746

Benavides, S. J., & Flierl, G. R. 2020, Journal of Fluid Mechanics, 900, A28, doi: 10.1017/jfm.2020.500

Burattini, P., Kinet, M., Carati, D., & Knaepen, B. 2008, Physics of Fluids, 20, 065110, doi: 10.1063/1.2940142

Cho, J. Y.-K. 2008, Philosophical Transactions of the Royal Society A: Mathematical, Physical and Engineering Sciences, 366, 4477

Cho, J. Y.-K., Menou, K., Hansen, B. M. S., & Seager, S. 2003, The Astrophysical Journal, 587, L117, doi: 10.1086/375016

Davidson, P. A. 1995, Journal of Fluid Mechanics, 299, 153, doi: 10.1017/S0022112095003466

—. 2013, Turbulence in rotating, stratified and electrically conducting fluids (Cambridge University Press)

Dobbs-Dixon, I., & Lin, D. N. C. 2008, The Astrophysical Journal, 673, 513, doi: 10.1086/523786

Ehrenreich, D., Lovis, C., Allart, R., et al. 2020, Nature, 580, 597

Favier, B., Godeferd, F. S., Cambon, C., & Delache, A. 2010, Physics of Fluids, 22, 075104, doi: 10.1063/1.3456725

Favier, B., Godeferd, F. S., Cambon, C., Delache, A., & Bos, W. J. T. 2011, Journal of Fluid Mechanics, 681, 434–461, doi: 10.1017/jfm.2011.207

Frisch, U. 1995, Turbulence: the legacy of AN Kolmogorov (Cambridge University Press)

Gallet, B., Berhanu, M., & Mordant, N. 2009, Physics of Fluids, 21, 085107, doi: 10.1063/1.3194304

Gallet, B., & Doering, C. R. 2015, Journal of Fluid Mechanics, 773, 154–177, doi: 10.1017/jfm.2015.232

Heng, K., Menou, K., & Phillipps, P. J. 2011, Monthly Notices of the Royal Astronomical Society, 413, 2380, doi: 10.1111/j.1365-2966.2011.18315.x

Heng, K., & Showman, A. P. 2015, Annual Review of Earth and Planetary Sciences, 43, 509, doi: 10.1146/annurev-earth-060614-105146

Heng, K., & Workman, J. 2014, The Astrophysical Journal Supplement Series, 213, 27, doi: 10.1088/0067-0049/213/2/27

Hindle, A. W., Bushby, P. J., & Rogers, T. M. 2019, The Astrophysical Journal Letters, 872, L27, doi: 10.3847/2041-8213/ab05dd

—. 2021, The Astrophysical Journal Letters, 916, L8, doi: 10.3847/2041-8213/ac0fec

Klein, R., & Pothérat, A. 2010, Phys. Rev. Lett., 104, 034502, doi: 10.1103/PhysRevLett.104.034502

Knaepen, B., & Moreau, R. 2008, Annual Review of Fluid Mechanics, 40, 25, doi: 10.1146/annurev.fluid.39.050905.110231

Knutson, H. A., Charbonneau, D., Allen, L. E., et al. 2007, Nature, 447, 183, doi: 10.1038/nature05782

Knutson, H. A., Charbonneau, D., Cowan, N. B., et al. 2008, The Astrophysical Journal, 690, 822, doi: 10.1088/0004-637x/690/1/822

Koll, D. D. B., & Komacek, T. D. 2018, The Astrophysical Journal, 853, 133, doi: 10.3847/1538-4357/aaa3de

Komacek, T. D., & Showman, A. P. 2016, The Astrophysical Journal, 821, 16, doi: 10.3847/0004-637x/821/1/16

Koskinen, T. T., Cho, J. Y., Achilleos, N., & Aylward, A. D. 2010, The Astrophysical Journal, 722, 178, doi: 10.1088/0004-637X/722/1/178

Koskinen, T. T., Yelle, R. V., Lavvas, P., & Cho, J. Y. 2014, The Astrophysical Journal, 796, doi: 10.1088/0004-637X/796/1/16

Kreidberg, L., Line, M. R., Parmentier, V., et al. 2018, The Astronomical Journal, 156, 17, doi: 10.3847/1538-3881/aac3df

Langton, J., & Laughlin, G. 2007, The Astrophysical Journal, 657, L113, doi: 10.1086/513185

Louden, T., & Wheatley, P. J. 2015, The Astrophysical Journal Letters, 814, L24, doi: 10.1088/2041-8205/814/2/l24

Menou, K. 2012, The Astrophysical Journal, 745, 138. http://stacks.iop.org/0004-637X/745/i=2/a=138

Menou, K., & Rauscher, E. 2009, The Astrophysical Journal, 700, 887, doi: 10.1088/0004-637x/700/1/887

Mininni, P. D., Rosenberg, D., Reddy, R., & Pouquet, A. 2011, Parallel Computing, 37, 316

Moffatt, H. K. 1967, Journal of Fluid Mechanics, 28, 571, doi: 10.1017/S0022112067002307

Perna, R., Menou, K., & Rauscher, E. 2010a, The Astrophysical Journal, 719, 1421, doi: 10.1088/0004-637X/719/2/1421

—. 2010b, The Astrophysical Journal, 724, 313. http://stacks.iop.org/0004-637X/724/i=1/a=313

Potherat, A., & Klein, R. 2017, Physical Review Fluids, 2

Pothérat, A., & Klein, R. 2014, Journal of Fluid Mechanics, 761, 168–205, doi: 10.1017/jfm.2014.620

Pouquet, A., Rosenberg, D., Stawarz, J., & Marino, R. 2019, Earth and Space Science, 6, 351, doi: https://doi.org/10.1029/2018EA000432

Rauscher, E., & Menou, K. 2010, The Astrophysical Journal, 714, 1334, doi: 10.1088/0004-637x/714/2/1334

—. 2012, The Astrophysical Journal, 750, 96, doi: 10.1088/0004-637x/750/2/96

—. 2013, The Astrophysical Journal, 764, 103, doi: 10.1088/0004-637x/764/1/103

Reddy, K. S., & Verma, M. K. 2014, Physics of Fluids, 26, 025109, doi: 10.1063/1.4864654

Reiners, A., & Christensen, U. R. 2010, A&A, 522, A13, doi: 10.1051/0004-6361/201014251

Rogers, T. M. 2017, Nature Astronomy, 1, 0131, doi: 10.1038/s41550-017-0131

Rogers, T. M., & Komacek, T. D. 2014, The Astrophysical Journal, 794, 132, doi: 10.1088/0004-637X/794/2/132

Rogers, T. M., & McElwaine, J. N. 2017, The Astrophysical Journal Letters, 841, L26, doi: 10.3847/2041-8213/aa72da

Rogers, T. M., & Showman, A. P. 2014, The Astrophysical Journal Letters, 782, L4, doi: 10.1088/2041-8205/782/1/l4

Seager, S. 2010, Exoplanets (University of Arizona Press)

Showman, A. P., Fortney, J. J., Lian, Y., et al. 2009, The Astrophysical Journal, 699, 564, doi: 10.1088/0004-637x/699/1/564

Showman, A. P., & Guillot, T. 2002, A&A, 385, 166, doi: 10.1051/0004-6361:20020101

Showman, A. P., & Polvani, L. M. 2011, The Astrophysical Journal, 738, 71, doi: 10.1088/0004-637x/738/1/71

Sommeria, J. 1988, Journal of Fluid Mechanics, 189, 553–569, doi: 10.1017/S0022112088001144

Sommeria, J., & Moreau, R. 1982, Journal of Fluid Mechanics, 118, 507–518, doi: 10.1017/S0022112082001177

Thess, A., & Zikanov, O. 2007, Journal of Fluid Mechanics, 579, 383–412

Verma, M. K. 2017, Rep. Prog. Phys., 80, 087001, doi: 10.1088/1361-6633/aa6c82

Yadav, R. K., & Thorngren, D. P. 2017, The Astrophysical Journal Letters, 849, L12, doi: 10.3847/2041-8213/aa93fd

Zellem, R. T., Lewis, N. K., Knutson, H. A., et al. 2014, The Astrophysical Journal, 790, 53, doi: 10.1088/0004-637x/790/1/53

Zikanov, O., & Thess, A. 1998, Journal of Fluid Mechanics, 358, 299–333, doi: 10.1017/S0022112097008239